Manuscript prepared for Atmos. Chem. Phys.
with version 2014/07/29 7.12 Copernicus papers of the LaTeX class copernicus.cls.
Date: 13 April 2017

Assessment of cloud related fine mode AOD enhancements based on AERONET SDA product

A. Arola[1], T.F. Eck[2,3], H. Kokkola[1], M. R. A. Pitkänen[1,4], and S. Romakkaniemi[1]

[1]Finnish Meteorological Institute, Kuopio, Finland.
[2]Universities Space Research Association, Columbia, MD, USA.
[3]NASA Goddard Space Flight Center, Greenbelt, MD, USA.
[4]Department of Applied Physics, University of Eastern Finland, Kuopio.

Correspondence to: Antti Arola
(antti.arola@fmi.fi)

Abstract.

AERONET (AErosol RObotic NETwork), which is a network of ground-based sun photometers, produces a data product called the Aerosol Spectral Deconvolution Algorithm (SDA) that utilizes spectral total aerosol optical depth AOD data to infer the component fine and coarse mode optical depths at 500nm. Based on its assumptions, SDA identifies cloud optical depth as the coarse mode AOD component and therefore effectively computes the fine mode AOD also in mixed cloud-aerosol observations. Therefore, it can be argued that the more representative AOD for fine mode fraction should be based on all direct sun measurements and not only on those cloud-screened for clear-sky conditions, in other words on those from Level 1 (L1) instead of Level 2 (L2) in AERONET. The objective of our study was to assess, including all the available AERONET sites, how the fine mode AOD is enhanced in cloudy conditions, contrasting SDA L1 and L2 in our analysis. Assuming that the cloud-screening correctly separates the cloudy and clear-sky conditions, then the increases in fine mode AOD can be due to various cloud-related processes, mainly by the strong hygroscopic growth of particles in the vicinity of clouds and in-cloud processing leading to growth of accumulation mode particles. We estimated these cloud-related enhancements in fine mode AOD seasonally and found, for instance, that in June-August season the average over all the AERONET sites was 0.011, when total fine mode AOD from L2 data was 0.154, therefore the relative enhancement was 7%. The enhancements were largest, both absolutely and relatively, in East-Asia; for example in June-August season the absolute and relative differences in fine mode AOD, between L1 and L2 measurements, were 0.022 and 10%, respectively. Corresponding values in North-America and Europe were about 0.01 and 6-7%. In some some highly polluted areas the enhancement is greater than these regional averages, e.g. in Beijing region and in JJA season the corresponding absolute values were about

0.1. It is difficult to separate the fine mode AOD enhancements due to in-cloud processing and hygroscopic growth, but we attempted to get some understanding by conducting a similar analysis for SDA-based fine mode Angstrom exponent (AE) patterns. Moreover, we exploited a cloud parcel model, in order to understand in detail the relative role of different processes. We found that in marine conditions, were aerosol concentration are low and cloud scavenging is efficient, the AE changes in opposite direction than in the more polluted conditions, were hygroscopic growth of particles leads to a negative AE change.

1 Introduction

Aerosol–cloud interactions contribute the largest uncertainty to the total anthropogenic radiative forcing (Myhre, 2013). One of the issues that hinder the measurement-based assessment of aerosol-cloud interactions by remote sensing methods is that typically aerosols and clouds cannot be measured simultaneously by passive remote sensing methods, including ground-based sun-photometers. In these techniques, so-called cloud-screening algorithms are therefore applied to provide aerosol optical depth (AOD) measurements for clear-sky conditions only. Due to this limitation, in aerosol-cloud interaction studies, aerosol and cloud properties have inherently different temporal sampling and therefore additional effects, e.g. impact of meteorology, have necessarily a possible influence in the derived correlations.

Many observational studies have found positive correlations between cloud fraction and AOD (Ignatov et al., 2005; Chand et al., 2012). However, as stressed above, with passive remote sensing the AOD measurements in cloudy conditions are not possible and thus these studies have to rely on cloud-screening technique and therefore the derived cloud aerosol relationships might be linked more to cloud contamination than to real physical processes. On the other hand, active remote sensing of aerosol from lidar measurements does not suffer similarly from this issue of cloud adjacency and these data have been analyzed as well for cloud aerosol interaction effects. Cloud–Aerosol Lidar and Infrared Pathfinder Satellite Observations (CALIPSO) lidar data over oceans have been investigated for the relationship between aerosol and clouds (e.g., Várnai and Marshak, 2011; Yang, 2015). These studies have shown a sharp increase in aerosol signal within 4 km towards clouds.

The physical mechanisms contributing to the positive correlation between AOD and cloudiness, in addition to unphysical contamination by undetected clouds, are mainly the following: hygroscopic growth of aerosol particles particles in the vicinity of clouds, different meteorological conditions with different aerosol properties when clouds are present, and in-cloud processing (e.g. sulfate or nitrate aerosol production). The role of these effects, particularly hygroscopic growth versus meteorological influence, has been debated (e.g., Mauger and Norris, 2007; Engström and Ekman, 2010). However, it is a challenging task to separate the influence of each factor and thus, they have remained poorly known. One of the challenges is related to the time scale of physical processes involved; for-

mation of aerosol mass in gas-to-particle processes occur in minutes in cloud droplets compared to days in cloudless air (sulfate formation as an example), and thus it would be highly important to have same temporal sampling of aerosol and cloud properties.

AERONET (AErosol RObotic NETwork), which is a network of ground-based sun photometers, includes also so-called Aerosol Spectral Deconvolution Algorithm (SDA) that utilizes spectral total extinction AOD data to infer the component fine and coarse mode optical depths at 500nm. Based on its assumptions, SDA identifies cloud optical depth as the coarse mode AOD component and therefore effectively computes the fine mode AOD also in mixed cloud-aerosol observations. Therefore, these measurements provide interesting insight into the simultaneous aerosol cloud measurements. More specifically, one can obtain and separate aerosol information in clear-sky and cloudy sky conditions, when clouds are thin enough that the direct sun measurements are possible. We use direct sun measurements in our analysis and sunphotometry can only measure maximum optical depth (OD) of about 7 for overhead sun and OD*m < 7 (where m=optical airmass) for increasing solar zenith angle. This is a basic upper AOD limitation of sunphotometer measurements in general, not just for AERONET, since the direct beam signal contribution nearly vanishes at this upper limit. Therefore the total OD (AOD + cloud OD) that can be monitored in cloudy conditions is limited to thin to thick cirrus, while the other cloud types have typically larger optical depths. These other cloud types typically have high enough temporal variability (in 15 seconds and 15 minutes), so that the triplet variance is too high for the measurements to pass to L2 (clear-sky) and it is often too high that they would be even included in L1 (they are not included if RMS of raw counts >16%). Since Cirrus is typically at an altitude higher than the aerosol layer there is usually no enhancement of AOD with such cirrus observations.

AERONET SDA product has been used to some extent, for instance to study rapid AOD increases in the vicinity of cumulus clouds (Eck et al., 2014); but nevertheless it has not been fully exploited yet and thus its unique features offer potential for additional interesting studies. In this paper, we present an analysis of cloud enhanced AOD measurements, based on AERONET SDA product. We selected the measurements from those time periods when Level 2 data are available which signifies good calibration and therefore high AOD accuracy, and also good instrument performance. Some of the sites were also selected for a more detailed analysis to demonstrate the usefulness of SDA data.

When aerosol climatologies, monthly AOD means or other statistics are formed, then Level 2 data of clear-sky measurements (excluding cloudy cases) are usually only included. This has to be definitely done with passive satellite measurements, in order to avoid cloud contamination in total AOD. However, this can lead to systematic biases due to the sampling; clear-sky conditions are related to particular type of weather patterns, while the excluded cloudy cases may differ systematically also in their aerosol loading. Therefore, we want to stress that by our analysis, we can now obtain a quantitative estimate for the fine mode AOD that is more representative for all-sky conditions and thus also for the enhancement due to these cloudy cases.

2 Data and Methods

2.1 AERONET measurements

AERONET (AErosol RObotic NETwork) is a globally distributed network of automatic sun and sky scanning radiometers that measure at several wavelengths, typically centered at 0.34, 0.38, 0.44, 0.50, 0.67, 0.87, 0.94, and 1.02 μm. Each band has a full width of approximately 0.010 μm at half maximum (FWHM), except for 0.34 μm and 0.38μm channels that have FWHM of 0.002 μm. All of these spectral bands are utilized in the direct Sun measurements, while four of them are used for the sky radiance measurements, 0.44, 0.67, 0.87 and 1.02 μm. Spectral aerosol optical depth (AOD) is obtained from direct sun measurements at high accuracy (0.01 to 0.02 for overhead sun, with the larger errors in the UV (Eck et al., 1999)). The inversion product includes other aerosol optical properties, such as single scattering albedo (SSA), refractive indices and the column integrated aerosol size distributions above the measurement site provided at the sky radiance wavelengths (Holben et al., 1998; Dubovik et al., 2000).

The ability of spectral deconvolution algorithm (SDA) to separate coarse and fine mode AOD, both in clear-sky and cloudy conditions, plays a key role in our analysis. O'Neill et al. (2001, 2002) developed SDA algorithm that utilizes spectral total extinction AOD data, with the assumption of bimodal aerosol size distributions, to infer the component fine and coarse mode optical depths. An additional fundamental assumption of the algorithm is that the coarse mode Angstrom exponent (AE) and its derivative are assumed to be -0.15 and zero, respectively. The Angstrom exponent and its spectral variation of measured total AOD (dAE/dlnWL) are the measurement inputs to the algorithm. These are determined from spectral AOD measurements at 5 wavelength: 380, 440, 500, 675, and 870 nm.

We applied several specific quality checks, in order to select the best quality SDA retrievals. We required that all 5 SDA wavelengths (380, 440, 500, 675, and 870 nm) were available in the Level 2 data and the L1 data were only utilized when L2 data were available within one-week time window, to rule out any instrumental problems. The possible outliers were removed according to the following criterion: Abs(AOD500nm-AODSDA500nm)>(0.02+AOD500nm*0.005). This is the same consistency check between measured AOD at 500 nm and SDA retrieved total AOD at 500 nm that is applied in the quality control checks for AERONET Level 1.5 data for SDA. Additionally, a consistency check of measured AOD compared to SDA retrieved total AOD at 500 nm was applied to both the L1 and L2 SDA data.

It is also noted that there are many internal quality assurance steps already in the regular AERONET processing that ensure the quality and usefulness of both data levels (Level 1 and Level 2). The direct sun measurement data are not included in the AERONET Level 1 data set if the variance of the raw signal is very high within the triplet sequence. The variance threshold applied is based on the root mean square (RMS) differences of the three direct sun triplet measurements relative to the mean

of these three values. If the (RMS/mean)·100% of the triplet values is greater than 16% then the data will not be used for computation of AOD and the data will not appear in the Level 1 data set. This temporal variance threshold primarily removes data that are affected by clouds with large spatial–temporal variance in cloud optical depth (COD). This effectively removes much of the cumulus cloud contaminated data, although some of the thinner edges with lower COD do remain in the data. In the AERONET Version 2 Level 2 database, if there are only 1 or 2 points remaining in a day after automatic cloud screening (Level 1.5), then none of this data reaches Level 2. In other words, at least 3 AOD observations are needed to pass the Smirnov et al. (2000) cloud screening algorithm in order for the data to reach Level 2 for that day. The Figure S1 in the supplement illustrates this in XiangHe site on August 10, 2010, when only two measurements remained after L1.5 cloud screening and those did not advance to L2 because AERONET requires a minimum of 3 points per day in L2.

2.2 AERONET data selection and analysis

In our analysis, we included fine mode AOD and AE at 500 nm, from both Level 1 and Level 2 SDA measurements, the former for all-sky conditions and the latter for clear-sky conditions. This data version (Version 2) includes cloud screening of Smirnov et al. (2000), which has been used for all papers using AERONET data since 2000 when this cloud screening algorithm was implemented. New version 3 will be released in 2017, with significantly different cloud screening.

Moreover, we constructed our own specific "Level 0" (L0) data set of SDA measurements, including only those cases of Level 1 that were not in Level 2, thus this set includes only cloudy cases, according to the cloud-screening. From these different data sets we calculated the monthly means as follows. First, we calculated hourly means and averaged them to obtain the daily averages. These daily mean values were then used to calculate the monthly averages, by requiring at least 10 days per month. For the seasonal means it was required that all the months had sufficient amount of measurements Figure S2 in the Supplement gives a histogram of the number of L0 vs. L2 measurements of all the sites included, indicating that most commonly the number in "cloudy-sky" (L0) data set is about 25% smaller than in the clear-sky (L2) data set. The "cloudy-sky" data is primarily direct sun observations in the near vicinity of clouds, not mainly the observation of aerosol through clouds. citeeck14 provides a detailed analysis of the AERONET cloud screening of these high temporal variance AOD observations near to clouds. The marine sites, on the other hand, seemed to have relatively a higher number of through cloud measurements in L0 data set; this will be discussed in more detail in the Section 3.2.

Eck et al. (2014) included several example cases to demonstrate how the AERONET Version 2 Level 1 data include meaningful information for our study as well. In their Figures 16c and 16d, Eck et al. (2014) showed AOD measurements at BLDND site for one day during DRAGON campaign indicating how the large triplet variation data, which is often screened from Level 2, is in fact good fine mode AOD data. As was shown by the MODIS images in Eck et al. (2014), the only cloud type

on this site and date was cumulus. Figure 1 shows this same case, but zooming into the afternoon measurements only and includes additionally both fine mode and total Angstrom exponents. During this time period when AOD increased substantially, the Angstrom exponent remained high and relatively constant indicating the dominance of small particles and no significant cloud contamination, the latter point is also supported by very small coarse mode AOD throughout the period.

The strength of SDA algorithm is that fine mode AOD can be obtained also in cloudy conditions, as demonstrated by O'Neill et al. (2002), since it identifies cloud optical depth as the coarse mode AOD component. Moreover, Chew et al. (2011), by comparing AERONET measured spectral AOD with lidar data, showed that SDA is able to effectively separate the fine and coarse so that the latter is only influenced by clouds. Additionally, Kaku et al. (2014) have verified that the SDA technique is also effective in separating the fine and coarse modes from in situ spectral optical measurements. It was shown by Eck et al. (2014) also that the AOD enhancements in the vicinity of cumulus clouds that were measured by AERONET direct sun measurements were also measured independently by lidar instruments (both surface and aircraft based) and by in situ measurements of aerosol properties from aircraft profiles in the vicinity of these clouds. These enhanced AOD measurements near cumulus are typically removed by AERONET cloud screening since the algorithm operates primarily on temporal variance of optical depth (assuming cloud optical depth has higher variability) and the turbulent and dynamic environment near to clouds sometimes results in high frequency variation of AOD.

It is likely, however, that the fine mode AOD is underestimated when cirrus ice crystal clouds overlay the aerosol, due to strong forward scattering into the field-of-view of the sun-photometer (A. Smirnov: personal communication, 2016). However cloud screening also occurs when cirrus is not present (high temporal variance in the presence of clouds ; Eck et al. (2014)) and also when very few AOD observations occur on a primarily cloudy day. Nonetheless, since some of the cloud observations occur with cirrus present, the SDA overall provides a lower limit on the enhancement of fine AOD in the presence of clouds. Figure S3 in the Supplement gives an example of one day measurements from GSFC, August 11, 2010, with cirrus clouds present in the afternoon. Non-cloud-screened measurements (L1) between 17-21 UTC illustrate how cloud contamination is in the coarse mode only and fine mode AOD measurements seem to be not cloud contaminated.

2.3 Cloud parcel model simulations

The numerical model employed here to study aerosol and cloud droplet microphysics is a so called cloud parcel model which has been described in detail in Kokkola et al. (2003); Romakkaniemi et al. (2006, 2009, 2011). In short, the model solves condensation and evaporation of water between the gas and particle phase. It has a sectional representation of aerosol particle size distribution with a detailed size dependent description of aerosol composition. The model can be employed to study how aerosol size distribution and composition are affecting the wet size of particles and cloud droplet formation in different atmospheric conditions.

For the cloud parcel model simulations the aerosol particle size distribution and composition as well as updraft velocity are needed as an input. In order to obtain the aerosol dry size distribution, we used the monthly mean AERONET-measured size distributions from the Level 2 inversion product. The size distributions from AERONET represent the ambient column averaged volume size distributions. To translate this into dry aerosol size distribution we need to make assumptions on the particle composition and vertical aerosol profiles. The first assumption is that all aerosol is residing in the boundary layer with a height of 1km. In reality this does not hold exactly, however the height of the layer is needed in order to estimate the aerosol number concentration from the columnar aerosol volume distribution. The change in the assumed boundary layer height will translate into change in the aerosol number concentration. The second assumption needed is for aerosol composition. As AERONET provides an estimate of aerosol volume distribution in ambient conditions, the aerosol hygroscopicity information is needed to approximate the dry aerosol size distribution from the wet (ambient) size distribution. Related to this, a value for relative humidity (RH) of air has to be assumed. Here we assume an effective RH in which the modeled wet aerosol size distribution is reproducing the observed AERONET- measured size distribution. Here different assumptions are not independent of each other. For example the change in effective RH could be balanced with a change in the particle dry size to produce similar wet size distribution as aerosol particles grow as a function of RH. This will be discussed in more detail in the results section

As an output, the cloud parcel model calculates the ambient size distribution of aerosol particles and cloud droplets at different altitudes. These size distributions are used as an input to Mie calculations, in order to obtain the extinction coefficient and the corresponding Angstrom exponents at each model level together with the integrated columnar estimates of AOD and AE. These calculations are carried out using the Mie calculation tool in LibRadtran (Mayer and Kylling, 2005) version 2.0, assuming purely scattering particles with the real part of refractive index of 1.5. The total column AOD and AE, as sun-photometer in AERONET network would measure from these modelled profiles, were estimated both for the cloudy and clear-sky case. In the latter case, the column AOD and AE values were integrated over the model calculated aerosol profile from the ground level up to a level where RH reached 3% higher value than effective RH that was used to determine the dry size distribution. This was estimated to correspond to the highest humidity in clear-sky conditions and it was found to approximately reproduce the observed AOD. The remaining layers above this level were integrated assuming that they have this constant extinction, thus estimating the contribution from cloud-free model levels as measured by AERONET.

3   Results

3.1   Spatial and temporal patterns of cloud induced AOD and AE

We conducted our analysis first for all the available AERONET sites on a seasonal basis, for the following seasons: March-May (MAM), June-August (JJA), September-November (SON), December-February (DJF). Figure 2 shows these seasonal cases of the difference in AOD between Level 0 and Level 2 data, thus between cases of solely cloudy or clear-sky AOD measurements. We additionally sub-divided our results into the following seven regions, shown also by lines in the plots: North-America, South-America, Europe, North-Africa, South-Africa, Asia, and Australasia. Table 1 shows the seasonal results for each region, e.g. the enhanced fine mode AOD, if sampled only for clear-sky conditions compared to cloudy-sky or all-sky cases. We can see that the AOD enhancements are consistently largest throughout the year in the Asia, reaching values of about 0.1 in many sites. This is a substantial difference that would not have a negligible effect in the radiative effect estimates either, if Level 2 data were used instead. On the other hand, the difference over all the included sites (values given in the Table 2) is rather notable as well, e.g. in JJA fine mode AOD of all-sky data is 0.011 higher than the mean based on Level 2 only (0.154), thus all-sky fine mode AOD being about 7% higher.

We also established the AOD differences on a monthly basis separately for each AERONET site. Moreover, we made it similarly for fine mode AE parameter, which was weighted by AOD. We considered this AOD weighting both necessary and useful, in order to produce more robust signal for the seasonality; otherwise the within month AE variability was substantially higher, clearly due to the cases of lowest AOD when the AOD magnitude approaches the uncertainty of the single channel AOD itself.

Figures 3 and 4 show examples of two sites (Walker Branch and Lanai), which will be studied in more detail also by cloud parcel modeling in the next section to understand some of the observed differences, while in the Supplement several other sites are included as well (Arica, Chile; Gwangju GIST, South Korea; Taihu and XiangHe, China). These figures show the monthly AOD-weighted dAE (difference in AE between Level 0 and Level 2 data) and the corresponding annual pattern of $dAOD$ (difference in AOD between Level 0 and Level 2).

Many of the sites exhibit a clear seasonality in $dAOD$ with highest enhancements around JJA season, for instance in Walker Branch, XiangHe, Gwangju GIST. Moreover, often the timing of the highest $dAOD$ is related to slightly negative dAE, perhaps most evidently in XiangHe and Walker Branch. In other words, AE of cloudy cases is slightly smaller, suggesting somewhat larger particles, likely related to swelling in humid conditions. However, these dAE differences are generally relatively small. As shown by Eck et al. (2014), for cumulus clouds in the mid-Atlantic US (Tselioudis et al., 2013) the dAE did not change much despite large changes in AOD on some days. This strongly suggested that particles grew in size from sub-visible Aitken, in addition to larger par-

ticle swelling in the high RH environment in and near clouds. In such a polluted environment (e.g. Baltimore-Washington region in Eck et al. (2014)) where it is known that there is SO2 present it is also highly likely that sulfate particle formation also occurs in the clouds (rapid SO2 to sulfate conversion in aqueous phase versus relatively slow in non-cloudy environments). Other gas-to-particle

275 conversions are likely in the aqueous phase in cloud droplets (nitrates and organic particles; (e.g., Hayden et al., 2008; Ervens et al., 2011)). Therefore near zero change in AE could mean both processes are counter-balancing each other.

The dAE differences are generally small and most often negative values. Moreover, these patterns of dAE do not show generally a strong seasonality. However, there were few sites having positive

280 differences systematically, mainly marine sites such as Lanai (Figure 4). The possible reasons for these cases are studied in more detail in the next section.

3.2 Cloud parcel model based investigation of cloud-induced AOD and AE changes.

The fine mode AE differences between cloudy and clear-sky cases shown in the previous section exhibited typically negative values. As discussed above, in these cases the particle growth is likely

285 a more dominant process than cloud activation. The latter process would remove the largest sizes, while the former results in an increase in the effective wet particle size. However, there were about ten sites with clearly positive dAE, all being either Island or coastal sites. As an example of such a case is the weighted fine mode dAE (Figure 4) observed at Lanai; the sixth-largest of the Hawaiian Islands. Although, these positive values are not very large, negative cases seem to be essentially

290 missing particularly during the summer.

Our main interest is to quantitatively understand the processes and their relative importance that could result in prevailing positive fine mode dAE. The sites with positive dAE, are all influenced by marine aerosol that typically has a strong bimodality with relatively small particles in the Aitken/accumulation mode, (e.g., Heintzenberg et al., 2004). With such aerosol size distribution

295 it is possible that the critical size for droplet formation reaches small enough particle sizes to affect the fine mode AOD. Thus the depletion of these particles into cloud droplets could decrease the effective size in the fine mode, being an opposing effect to the growth of aerosols by humidity.

By employing the numerical cloud parcel model, we investigated in more detail the relative role of aerosol hygroscopic growth and cloud activation on the enhancement of AOD and how this can affect

300 the observed AE. This was done for contrasting conditions, namely Lanai and Walker Branch that represent completely different aerosol conditions. For simplicity we assumed the Lanai aerosol to be solely composed of NaCl to represent highly hygroscopic sea salt aerosol. For Walker Branch, the composition was assumed to be 50% insoluble organics and 50% inorganic ammonium sulfate. This composition is assumed to be representative of continental aerosol. For the aerosol size distributions

305 we used AERONET observed monthly mean size distributions from the Level2 inversion product for August 2003.

Apart from the initial size and composition distribution, the initial conditions were assumed to be the same in all simulations: ambient temperature of 288 K and RH of 63 %. After the initialization, model simulated cloud formation for an adiabatically ascending air parcel with a constant updraft velocity w. In Lanai, w was assumed to be $0.2\,\mathrm{m\,s^{-1}}$ which is quite typical for marine stratocumulus clouds. In Walker Branch w was assumed to be $0.5\,\mathrm{m\,s^{-1}}$, which is typical to broken small cumulus clouds. In the simulations the boundary height was assumed to be 1 km. Assuming that the air parcel ascends adiabatically, the cloud base was reached at 880 m resulting in cloud height of 120 m.

From the simulated wet size distributions, we calculated the optical properties of the aerosol/cloud droplet population for different altitudes. This was done for both Walker Branch (WB) and Lanai aerosol size distributions, with more detailed examination of Lanai case. The numbers within Figure 5 are given for the simulations of two different cases of growth factors (the ratio between the wet and dry diameter) in Lanai, as an estimate of the AERONET-measurement from these profiles in a manner explained in methods section. For example, the first three numbers are for the case of growth factor of 2 as follows: AOD of clear-sky profile, "$AODL2$"; AOD difference between cloudy and clear-sky profiles, "$dAOD1$"; AE difference between cloudy and clear-sky profile, "$dAE1$". The next three numbers correspond similarly to the case of increased growth factor of 2.2, indicating a positive value for dAE and a change of sign if compared to the case with growth factor of 2.

This result of positive dAE was achieved with an aerosol size distribution which reproduced observed AERONET distribution at 85 % relative humidity, where the growth factor of particles composed of NaCl is approximately 2.2 (see Figure 1 of Ming and Russell (2001)). To illustrate the effect of hygroscopicity on the aerosol optical properties, we used also another dry size distributions for Lanai: one, where the dry size distribution reproduced the AERONET-observed ambient size distribution at 80 % relative humidity, where the growth factor is approximately 2. Thus, in the latter case, the dry size required to reproduce the AERONET observations was slightly larger than in the case of 85 %. This will directly affect also the wet size of fine mode particles in the cloud, where the growth factor of NaCl particles is between 4-5 depending on the particle size and supersaturation, and now the sign of dAE changed.

These simulations demonstrate that dAE can indeed turn to a positive value, but only for highly hygroscopic NaCl aerosols, and when the particle dry sizes are sufficiently small and the supersaturation at the cloud base is high enough to activate these particles. In such a case the largest interstitial aerosol particles are clearly smaller than the estimated size limit for fine mode aerosol classification. For less hygroscopic aerosol composition and higher total aerosol concentration, e.g. the one we assumed for our Walker Branch simulations, did not produce positive dAE cases. In Lanai, the activation of smaller particles than in Walker Branch was further assisted by low number concentration and small dry sizes of aerosol which allowed the maximum supersaturation to reach higher values.

Based on our model simulations, it seems evident that cloud activation can affect and remove particles from the AERONET-measured fine mode AOD, resulting in positive dAE between L0 and

L2 measurements. We wanted to additionally assess this threshold of activation size that needs to be

345 reached, so that the effect of the removal of the cloud activated largest size particles in the fine mode, would overcome the hygroscopic growth of the smaller particles in the case of marine aerosol size distribution observed in Lanai. The former process has the overall effect to increase AE in cloudy case, while the latter has an opposing effect. The upper plot of Figure 6 shows the cloud activation (critical) radius as a function critical supersaturation. We repeated our Mie simulations for a range

350 of critical supersaturation from 0 to 0.3%, always removing particles larger than the critical radius corresponding to the critical supersaturation from the aerosol size distribution. The lower panel in Figure 6 shows dAE as a function critical supersaturation. The figure illustrates that only a relatively narrow range of critical supersaturation, corresponding to critical radius of about 0.3 μm, results in positive AE difference between cloudy and clear-sky column. With higher supersaturations, such

355 small particles are able to activate that the interstitial aerosol is no longer affecting column AOD and thus AE. At low supersaturations, the hygroscopic growth of interstitial particles dominates the column AE, and thus the influence of a cloud scavenging of particles results in negative dAE.

There are cloud related processes that our model simulations do not fully describe, including gas-to-particle conversion and chemical reactions occurring in the aqueous phase. These processes would

360 increase the distance between Aitken and accumulation mode, and thus likely magnify the modelled positive change in AE. In addition, the particle growth in humid regions in surrounding clouds is not included in our 1-D exercise. However, arguably the most important processes of marine cloud environment are included by our cloud parcel modeling study.

Figure 7, in turn, shows the results from our simulations in more detail for several cases. The sim-

365 ulations of both Walker Branch and Lanai are shown for two different model levels, e.g. WB@820 refers to the Walker Branch simulation at the model altitude of 820m, i.e. below the cloud base. To illustrate the effect of cloud activation on the fine mode, results close to the cloud top at 970 m are also shown ("Lanai@970" and "WB@970" for Lanai and Walker Branch, respectively). Finally, for the case of Lanai and close to the cloud top, we included two cases of different aerosol dry sizes, as

370 discussed above and were shown in the Figure 5. The left-hand-side y-axis shows these cases and the total particle area.

We also estimated AE for a range of single effective sizes by assuming a narrow log-normal size distribution (with the geometric standard deviation of 1.08) to represent a mono-disperse case for a size range up to 0.6 μm, this is shown by a black line corresponding to the right-hand-side y-axis.

375 This AE estimate was calculated from our modeled extinction efficiencies at 500nm and 340nm. Since the extinction efficiency multiplied by the total particle area gives the total extinction, this choice of plots in RHS and LHS y-axes gives an opportunity to assess the impact of different particle sizes in the total AE, with the following interpretation. The relative contribution from any single particle size to total AE can be estimated from mono-disperse AE weighted by the total particle area

380 of this given particle size.

At 820 m cloud activation has not affected the fine mode size distribution while higher in the cloud at 970 m particles larger than the activation diameter have been removed from the fine mode. The activation diameter in the Walker Branch simulation is at around 0.4 μm (red solid line) and it is smaller for our two Lanai cases (blue and green solid lines). As demonstrated in Figure 5, the growth factor of 2.2 was required for our NaCl simulation to produce positive dAE. And indeed with the help of the Figure 5 this can be understood, if we think about total AE as a convolution between mono-disperse AE and particle total area over particle sizes. For instance, convolution between black line and blue line for our Lanai case with the growth factor of 2. The lower the activation limit the lower is the contribution from sizes with negative AE, and thus larger is the total AE. The green line case, with the growth factor of 2.2, has reached low enough activation size to produce large enough AE for cloudy case and thus also positive dAE as was shown in the Figure 5.

4 Conclusions

The studies of aerosol–cloud interactions, exploiting remote sensing measurements, are challenging and therefore many aspects have remained poorly known. Typically the aerosol optical properties can be measured by passive remote sensing approaches only for clear-sky conditions. Active remote sensing (mainly Lidar) does not suffer equally about cloud adjacency effects, however the coverage that one can reach currently by active remote sensing is more limited. There exists one remote sensing product, so called spectral deconvolution (SDA) from AERONET, that can offer a unique information about the cloud effect on AOD. Therefore, it is somewhat surprising that these data have not been yet fully exploited for this purpose. We analyzed SDA for different cloud conditions to give quantitative estimates for the cloud enhanced AOD values, using all the available AERONET sites.

We performed the analysis on a seasonal basis and found that regardless of the season the highest cloud related AOD enhancements occur in East-Asia, reaching levels of AOD of about 0.1. In relative terms, these values are in range of 10-12% higher if compared to clear-sky (Level 2) fine mode AOD. This is not insignificant and should be taken into account for, e.g. in the calculations of aerosol radiative effects. On the other hand, the difference over all the included sites is rather notable as well, e.g. in JJA fine mode AOD of all-sky data is 0.011 higher than the mean based on Level 2 only (0.154), thus all-sky fine mode AOD being about 7% higher.

We estimated similarly the differences in fine mode AE, between cloudy- and clear-sky cases. In majority of the cases, negative AE differences were typically prevailing. These cases are likely dominated by particle growth in the humid conditions over the cloud activation. There were only about ten sites of clearly positive dAE, all being strongly affected by marine aerosols. It is noted that the AE changes were rather small, only few percent. Small new accumulation particles from both growth of Aitken sized particles and gas-to-particle conversion may counterbalance humidification growth of some existing accumulation mode particles, thereby resulting in little change in AE. However,

a more detailed analysis with a better information on aerosol composition is needed to explore the strength of competing effects.

Albeit overall dAE was small, in the marine cases the negative dAE cases were essentially missing, thus suggesting that different processes dominate if compared to the continental cases. Therefore, we investigated in more detail, with the help of cloud parcel model, the relative role of aerosol hygroscopic growth and cloud activation in different cloudy conditions. Our model simulations demonstrated that cloud activation can affect and remove particles from the AERONET-measured fine mode AOD, resulting in positive dAE between L0 and L1 measurements. However, this requires highly hygroscopic aerosol composition (sea salt) with sufficiently small dry sizes.

Acknowledgements.

References

Chand, D., R. Wood, S. J. Ghan, M. Wang, M. Ovchinnikov, P. J. Rasch, S. Miller, B. Schichtel, and T. Moore, Aerosol optical depth increase in partly cloudy conditions, J. Geophys. Res., 117, D17207, doi:10.1029/2012JD017894, 2012.

Chew, B. N., Campbell, J. R., Reid, J. S., Giles, D. M., Welton, E.J., Salinas, S. V., and Liew, S. C.: Tropical cirrus cloud contamination in sun photometer data, Atmos. Environ., 45, 6724–6731, doi:10.1016/j.atmosenv.2011.08.017, 2011.

Dubovik, O., A. Smirnov, B. N. Holben, M. D. King, Y. J. Kaufman, T. F. Eck, and I. Slutsker, Accuracy assessment of aerosol optical properties retrieval from AERONET sun and sky radiance measurements, J. Geophys. Res., 105, 9791–9806, 2000.

Eck, T., Holben, B., Reid, J. S., Dubovik, O., Smirnov, A., O'Neill, N. T., Slutsker, I., and Kinne, S., Wavelength dependence of the optical depth of biomass burning urban and desert dust aerosols, J. Geophys. Res., 104, 31333–31349, doi:10.1029/1999JD900923, 1999.

Eck, T. F., Holben, B. N., Reid, J. S., Arola, A., Ferrare, R. A., Hostetler, C. A., Crumeyrolle, S. N., Berkoff, T. A., Welton, E. J., Lolli, S., Lyapustin, A., Wang, Y., Schafer, J. S., Giles, D. M., Anderson, B. E., Thornhill, K. L., Minnis, P., Pickering, K. E., Loughner, C. P., Smirnov, A., and Sinyuk, A.: Observations of rapid aerosol optical depth enhancements in the vicinity of polluted cumulus clouds, Atmos. Chem. Phys., 14, 11633-11656, doi:10.5194/acp-14-11633-2014, 2014.

Engström, A., and A. M. L. Ekman, Impact of meteorological factors on the correlation between aerosol optical depth and cloud fraction, Geophys. Res. Lett., 37, L18814, doi:10.1029/2010GL044361, 2010.

Ervens, B., Turpin, B. J., and Weber, R. J.: Secondary organic aerosol formation in cloud droplets and aqueous particles (aqSOA): a review of laboratory, field and model studies, Atmos. Chem. Phys., 11, 11069–11102, doi:10.5194/acp-11-11069-2011, 2011.

Hayden, K. L., Macdonald, A. M., Gong, W., Toom-Sauntry, D., Anlauf, K. G., Leithead, A., Li, S.-M., Leaitch, W. R., and Noone, K.: Cloud processing of nitrate, J. Geophys. Res., 113, D18201, doi:10.1029/2007JD009732, 2008.

Heintzenberg, J., W. Birmili, A. Wiedensohler, A. Nowak, and T. Tuch, Structure, variability and persistence of the submicrometre marine aerosol. Tellus B, 56: 357–367, doi: 10.1111/j.1600-0889.2004.00115.x, 2004.

Holben B.N., T.F. Eck, I. Slutsker, D. Tanre, J.P. Buis, A. Setzer, E. Vermote, J.A. Reagan, Y. Kaufman, T. Nakajima, F. Lavenu, I. Jankowiak, and A. Smirnov, AERONET - A federated instrument network and data archive for aerosol characterization, Rem. Sens. Environ., 66, 1-16, 1998.

Ignatov, A., Minnis, P., Loeb, N., Wielicki, B., Miller, W., Sun-Mack, S., Tanre, D., Remer, L., Laslo, I., and Geier, E.: Two MODIS aerosol products over ocean on the Terra and Aqua CERES SSF., J. Atmos. Sci., 62, 1008–1031, 2005.

Kaku, K. C., Reid, J. S., O'Neill, N. T., Quinn, P. K., Coffman, D.J., and Eck, T. F.: Verification and application of the extended spectral deconvolution algorithm (SDA+) methodology to estimate aerosol fine and coarse mode extinction coefficients in the marine boundary layer, Atmos. Meas. Tech., 7, 3399–3412, doi:10.5194/amt-7-3399-2014, 2014.

Kokkola, H., Romakkaniemi, S., and Laaksonen, A.: A one-dimensional cloud model including trace gas condensation and sulfate chemistry, Boreal Env. Res., 8, 413–424, 2003.

Mayer B and A. Kylling, Technical note: The libRadtran software package for radiative transfer calculations - description and examples of use, Atmospheric Chemistry and Physics, 5, 1680-7324/acp/2005-5-1855, 1855-1877, 2005.

Ming, Y., and L. M. Russell, Predicted hygroscopic growth of sea salt aerosol, J. Geophys. Res., 106(D22),
470   28259–28274, doi:10.1029/2001JD000454, 2001.

Myhre, G., D. Shindell, F.-M. Bréon, W. Collins, J. Fuglestvedt, J. Huang, D. Koch, J.-F. Lamarque, D. Lee, B. Mendoza, T. Nakajima, A. Robock, G. Stephens, T. Takemura and H. Zhang, Anthropogenic and Natural Radiative Forcing. In: Climate Change 2013: The Physical Science Basis. Contribution of Working Group I to the Fifth Assessment Report of the Intergovernmental Panel on Climate Change [Stocker, T.F., D. Qin,
475   G.-K. Plattner, M. Tignor, S.K. Allen, J. Boschung, A. Nauels, Y. Xia, V. Bex and P.M. Midgley (eds.)]. Cambridge University Press, Cambridge, United Kingdom and New York, NY, USA, 2013.

Nenes, A., S. Ghan, H. Abdul-razzak, P. Chuang, and J. H. Seinfeld, Kinetic limitations on cloud droplet formation and impact on cloud albedo. Tellus Series B: Chemical and Physical Meteorology, 53, 133-149, doi:10.1034/j.1600-0889.2001.d01-12.x, 2001.

480   Mauger, G. S., and J. R. Norris, Meteorological bias in satellite estimates of aerosol-cloud relationships, Geophys. Res. Lett., 34, L16824, doi:10.1029/2007GL029952, 2007.

Romakkaniemi, S., Kokkola H., Lehtinen K.E.J., and Laaksonen A.: The influence of nitric acid on the cloud processing of aerosol particles, Atmos. Chem. Phys, 6, 1627-1634, 2006

Romakkaniemi, S., G. McFiggans, K.N. Bower, P. Brown, H. Coe, and T.W. Choularton: A comparison be-
485   tween trajectory ensemble and adiabatic parcel modelled cloud properties and evaluation against airborne measurements, J. Geophys. Res., doi:10.1029/2008JD011286, 2009

Romakkaniemi S., H. Kokkola, J.N. Smith, N.L. Prisle, A.N. Schwier, V.F. McNeill, A. Laaksonen: Partitioning of semivolatile surface active compounds between bulk, surface and gas phase, Geophys. Res. Lett., 38, L03807, doi:10.1029/2010GL046147, 2011

490   O'Neill, N. T., Eck, T. F., Holben, B. N., Smirnov, A., Dubovik, O., and Royer, A.: Bimodal size distribution influences on the variation of Angstrom derivatives in spectral and optical depth space, J. Geophys. Res., 106, 9787–9806, 2001.

O'Neill, N. T., Eck, T. F., Smirnov, A., Holben, B. N., and Thulasiraman, S.: Spectral discrimination of coarse and fine mode optical depth, J. Geophys. Res., 108, 4559, doi:10.1029/2002JD002975, 2003.

495   Smirnov, A., Holben, B. N., Eck, T. F., Dubovik, O., and Slutsker, I.: Cloud screening and quality control algorithms for the AERONET data base, Remote Sens. Environ., 73, 337–349, 2000.

Tselioudis, G., W. Rossow, Y.-C. Zhang, and D. Konsta, Global weather states and their properties from passive and active satellite cloud retrievals. J. Climate, 26, 7734-7746, doi:10.1175/JCLI-D-13-00024.1, 2013.

Várnai, T. and Marshak, A.: Global CALIPSO Observations of Aerosol Changes Near Clouds, IEEE, Geosci.
500   Remote Sens. Lett., 8, 19–23, 2011.

Yang, W., A. Marshak, T. Várnai, and R. Wood, CALIPSO observations of near-cloud aerosol properties as a function of cloud fraction, Geophys. Res. Lett., 41, 9150–9157, doi:10.1002/2014GL061896, 2015.
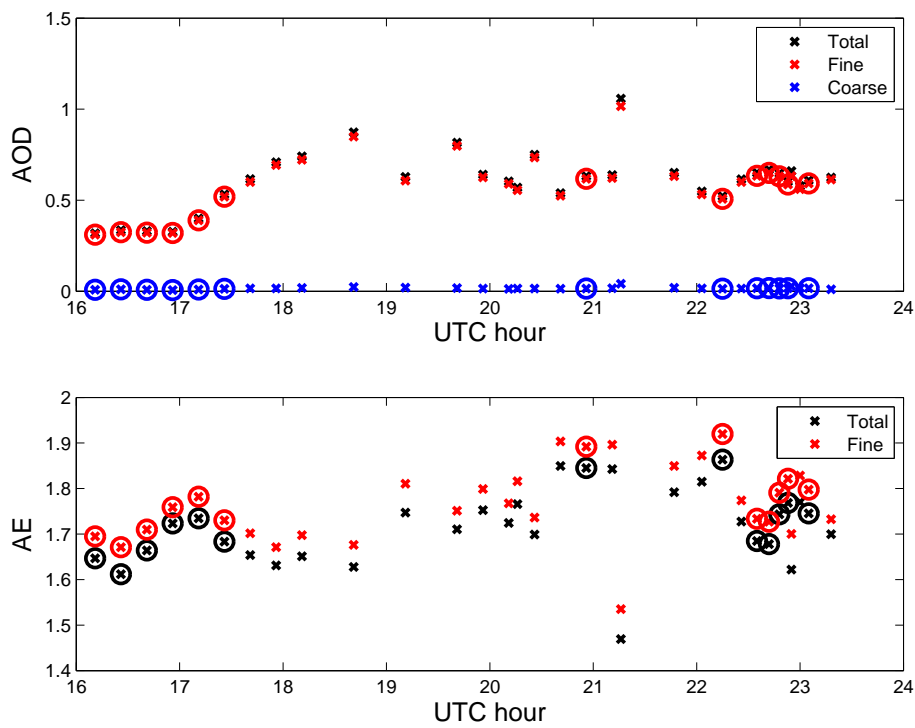
Figure 1. AOD (upper plot) and Angstrom exponent (lower plot) in BLDND site near Essex July 5, 2011. Red, blue and black symbols are for fine mode, coarse mode and total, respectively. Level 1 and Level 2 measurements are indicated by cross and circle, respectively.
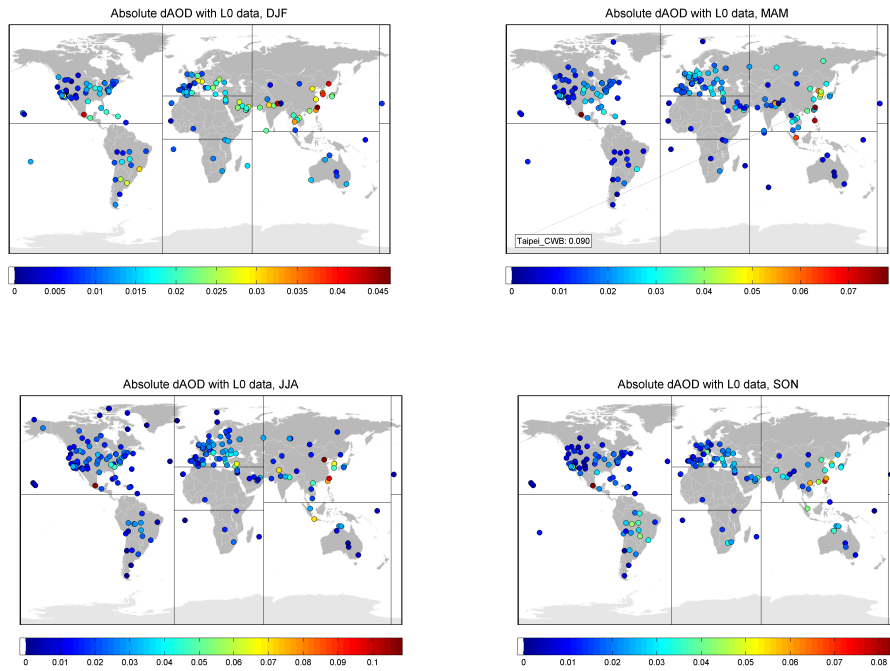
Figure 2. The difference between cloudy-sky and clear-sky (between L0 and L2) fine mode AOD for different seasons: DJF (in the upper left corner), MAM (in the upper right corner), JJA (in the lower left corner), and SON (in the lower right corner).
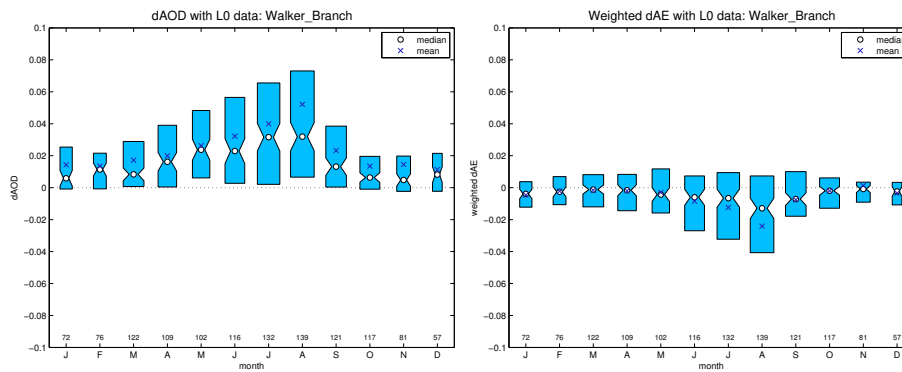
Figure 3. Monthly $dAOD$ and dAE (difference in L0 AE and L2 AE) for Walker Branch, TN, USA. Numbers at the bottom of the figure indicate the amount of measurements per month included in the box-plot.
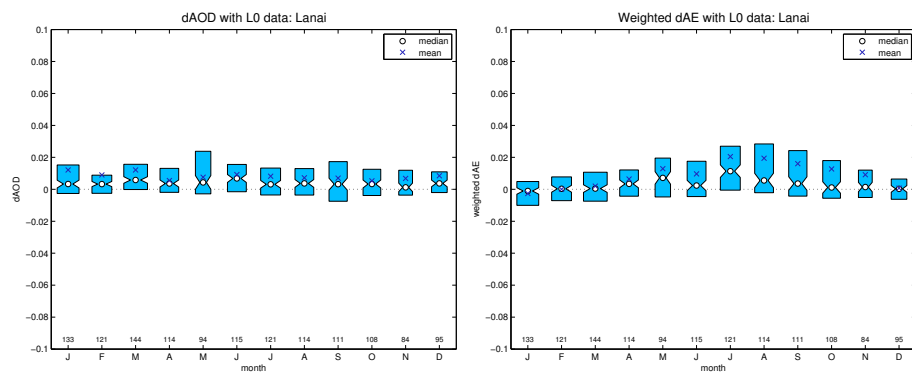
Figure 4. Similar to Figure 3, but for Lanai, Hawaii, USA.
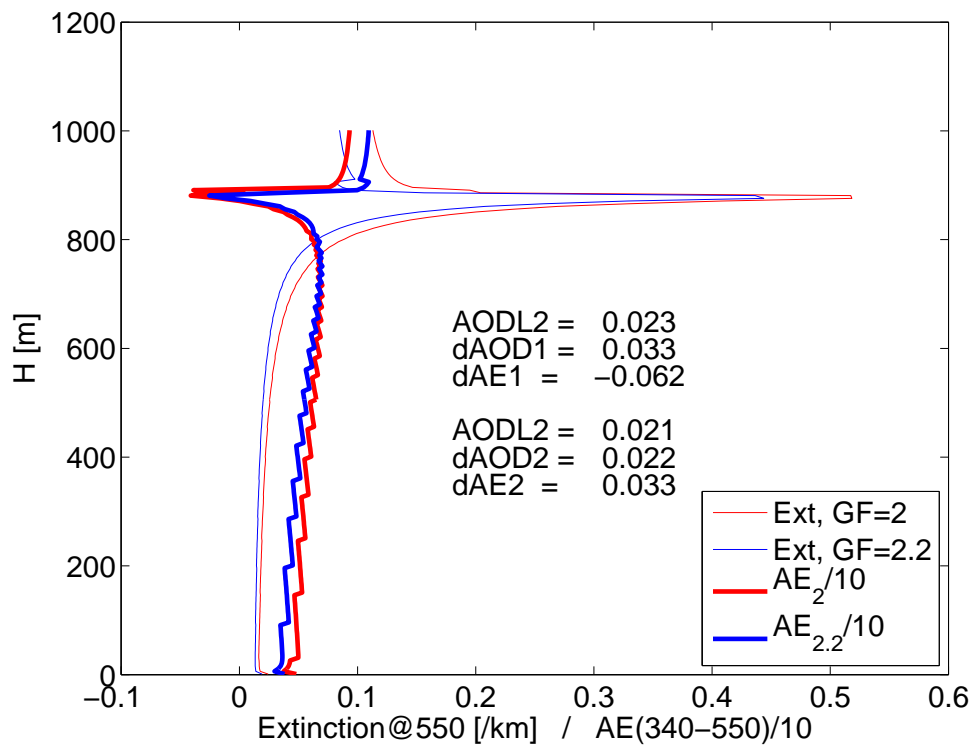
Figure 5. Profile of extinction at 500nm and Angstrom exponent from 340-500nm wavelength pair. The latter is divided by 10, in order to better match the x-scale. The numbers within the figure are given for the simulations of two different cases of growth factors (2 and 2.2). The first three numbers are for the case of growth factor of 2 as follows: AOD of clear-sky profile, "$AODL2$"; AOD difference between cloudy and clear-sky profiles, "$dAOD1$"; AE difference between cloudy and clear-sky profile, "$dAE1$". The next three numbers correspond similarly to the case of increased growth factor of 2.2,
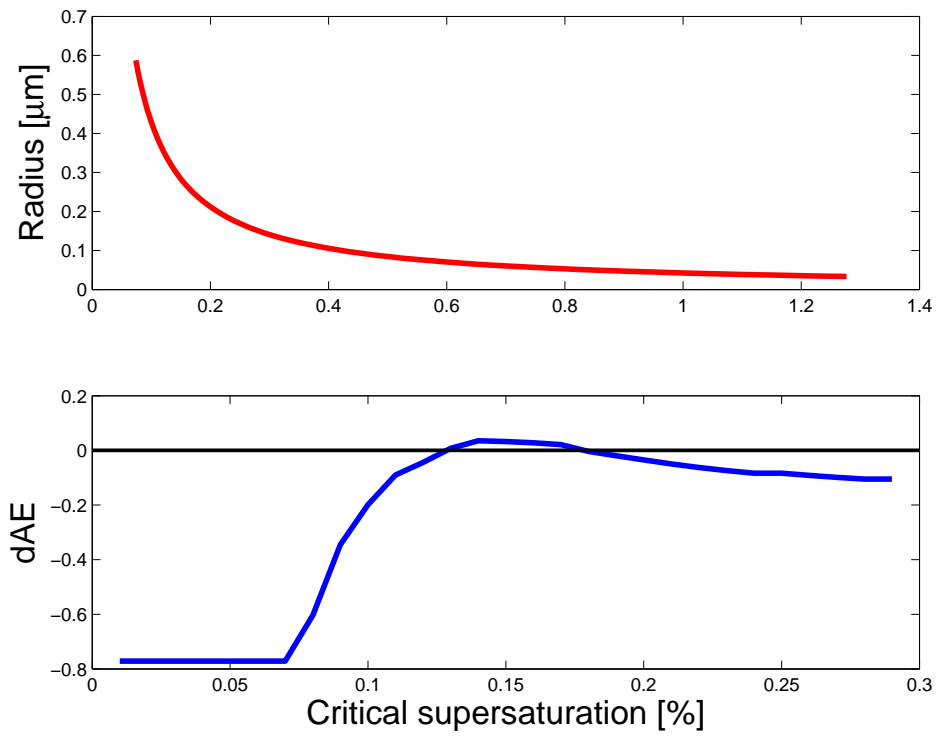
Figure 6. Critical cloud droplet activation radius as a function of critical supersaturation (upper plot) and esti-
mated difference in AE, between cloudy- and clear-sky case (lower plot).
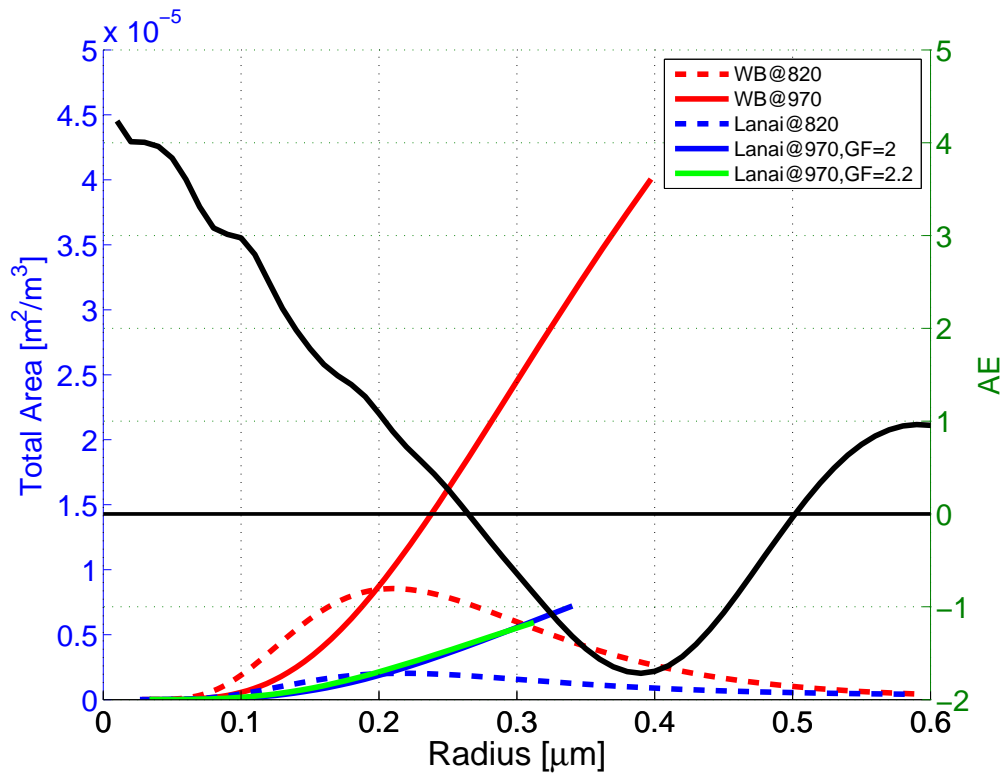
Figure 7. Total aerosol area per volume (LHS y-axis) at different model levels, WB refers to Walker Branch, e.g. WB@820 means Walker Branch case and altitude of 820m. Lanai is shown for two growth factors, 2 and 2.2, as discussed in more details in the text. RHS y-axis shows Angstrom exponent, as a estimated for mono-disperse aerosol of given radius.

Table 1. Seasonal AOD based on sampling for different cloudiness. L1 and L2 refer to Level 1 and Level 2 of AERONET data, respectively. L0 refers to those cases of L1, which did not belong to L2, thus cloudy cases only. Different regions have the following abbreviations: NAm (North America), SAm (South America), Eu (Europe), NAf (North Africa), SAf (South Africa), As (Asia), Aus (Australasia). These regions are indicated by the solid lines in the Figure 2.

NAm					SAm			
AOD	DJF	MAM	JJA	SON	DJF	MAM	JJA	SON
L1	0.052	0.096	0.147	0.078	0.088	0.065	0.126	0.249
L2	0.047	0.088	0.137	0.073	0.074	0.057	0.119	0.237
L0	0.059	0.105	0.158	0.087	0.095	0.071	0.139	0.262
d12	+0.005	+0.008	+0.010	+0.005	+0.014	+0.008	+0.007	+0.012
d02	+0.012	+0.017	+0.021	+0.014	+0.020	+0.014	+0.020	+0.025

Eu					NAf			
AOD	DJF	MAM	JJA	SON	DJF	MAM	JJA	SON
L1	0.092	0.137	0.152	0.108	0.124	0.112	0.146	0.138
L2	0.089	0.129	0.144	0.103	0.120	0.108	0.142	0.134
L0	0.101	0.149	0.168	0.118	0.136	0.122	0.159	0.153
d12	+0.003	+0.008	+0.009	+0.005	+0.005	+0.004	+0.004	+0.004
d02	+0.013	+0.020	+0.025	+0.015	+0.016	+0.014	+0.017	+0.019

SAf					As			
AOD	DJF	MAM	JJA	SON	DJF	MAM	JJA	SON
L1	0.126	0.084	0.141	0.168	0.289	0.319	0.262	0.268
L2	0.101	0.074	0.135	0.160	0.278	0.304	0.240	0.254
L0	0.139	0.092	0.150	0.174	0.303	0.332	0.273	0.282
d12	+0.026	+0.010	+0.006	+0.008	+0.011	+0.015	+0.022	+0.014
d02	+0.038	+0.018	+0.015	+0.014	+0.025	+0.029	+0.033	+0.028

Aus			
AOD	DJF	MAM	JJA	SON
L1	0.095	0.093	0.110	0.140
L2	0.085	0.083	0.099	0.129
L0	0.102	0.098	0.118	0.148
d12	+0.010	+0.010	+0.011	+0.011
d02	+0.016	+0.016	+0.019	+0.019

Table 2. Otherwise similar to Table 1, but showing overall results for all the sites.

All sites				
AOD	DJF	MAM	JJA	SON
L1	0.119	0.145	0.165	0.143
L2	0.112	0.136	0.154	0.135
L0	0.128	0.155	0.178	0.154
d12	+0.007	+0.009	+0.011	+0.008
d02	+0.016	+0.020	+0.024	+0.018